Journal of Alloys and Compounds 735 (2018) 2675–2684

Contents lists available at ScienceDirect

Journal of Alloys and Compounds

journal homepage: http://www.elsevier.com/locate/jalcom

Numerical simulation of the effect of aluminum foam on sorption induced wall strain in vertical, metal hydride based hydrogen storage container

Sidharth Shaji, G. Mohan*

Center for Computational Research in Clean Energy Technologies, Sree Chitra Thirunal College of Engineering, Thiruvananthapuram, Kerala, India

ARTICLE INFO

Article history:
Received 12 January 2017
Received in revised form
23 November 2017
Accepted 25 November 2017

Keywords:
Metal hydride
Aluminum foam
Wall strain
Hydrogen storage
Simulation

ABSTRACT

Low thermal conductivity of metal hydride alloys significantly affects the sorption performance of hydrogen storage devices. Upon hydrogenation they also exert significant stresses on the containers due to volume changes and thermal cycling. Aluminum foam has been widely accepted as a means to enhance heat transfer and thereby improve sorption performance of metal hydride storage devices. In addition to this, such foams can also serve to homogenize the container strains. In this study, numerical simulation of the wall strain development upon hydrogenation of a vertically aligned metal hydride storage device is performed. The device contains $LaNi_5$ as the storage alloy embedded with aluminum foam. Role of aluminum foam on hydrogenation and consequent development of wall strains is studied. Effect of controlled spatial variation of foam density as a means for strain reduction is also investigated.

1. Introduction

Safe storage of hydrogen at high gravimetric/volumetric storage capacity is one of the major requirements to be met for the realization of hydrogen economy. Solid state hydrogen storage devices using intermetallics and complex hydrides offer some noted benefits over their compressed and liquefied counterparts in terms of safety as well as volume and energy requirements. However system weight, durability and operability of these devices need improvement to make them practically viable.

Heat transfer is the dominant factor influencing sorption rate for metal hydrides. In addition to this, hydrogenation of these alloys induces significant lattice volume expansion which can lead to fragmentation of hydride particles. Subsequent to this, fine particles settle at the bottom and eventually agglomerate under the prevailing high pressure and temperature. Whole of these phenomena induce strains in the container wall and if left unaddressed while designing, can lead to significant distortions or failure.

A comprehensive review on heat and mass transfer of metal hydride beds was reported by Srinivasa Murthy et al. [1]. Majority of the numerical studies deals with 2D conservation equations with appropriate correlations for sorption kinetics. In its more conservative form, investigators [2,3] reported distinct equations of mass and energy for both gas and solid phases. More precise models also treated thermal conductivity as appropriate functions of bed porosity, hydride concentration, and temperature. Mohan et al. [4] investigated the hydriding performance of alloy bed embedded with multiple heat exchanger tubes. This study had shown the relevance of bed thickness, gas pressure and cooling fluid temperature on hydrogenation rate. Garrison et al. [5] studied the relevance of tube spacing and tube diameter on the optimal design of such devices.

Few studies were also reported on the mechanical characteristics of solid state hydrogen storage reactors. Okumura et al. [6] showed that hydride particles resulting from the pulverization of the alloy settle to the bottom of the reactor and effectively reduces the porosity in this region. McKillip et al. [7] and Nasako et al. [8] studied the wall strains in the container and showed that the high strains near the container bottom is attributed to the lower porosity in those regions. Ao et al. [9] found that these wall strains vary with hydrogen loading and cycle number. Most studies dealing with mechanical behaviour have not dealt with the effect of heat transfer on wall strain development. Lekshmi and Mohan [10] reported the effect of relevant parameters such as bed thickness, supply pressure of hydrogen and temperature of cooling fluid on

* Corresponding author.
E-mail address: mohan.g.menon@sctce.ac.in (G. Mohan).

https://doi.org/10.1016/j.jallcom.2017.11.289
0925-8388/

Nomenclature

b	bed thickness, m
B	shape factor
c	concentration of hydride, mol m^{-3}
C_p	specific heat, J kg^{-1} K^{-1}
E	activation energy, J mol^{-1}
F	reacted fraction
ΔH^0	heat of formation, J kg^{-1}
h	height, m
$\dot{m}$	rate of hydrogen absorbed, kg m^{-3} s^{-1}
P	pressure, Pa
r	radial coordinate, m
R	universal gas constant, J mol^{-1} K^{-1}
t	time, s
T	temperature, K
U	heat transfer coefficient, W m^{-2} K^{-1}
Y	Young's modulus, Pa
z	axial coordinate, m

Greek letters

β	deformed factor
ε	strain, μm m^{-1}
λ	thermal conductivity, W m^{-1} K^{-1}
ρ	density, kg m^{-3}
σ	stress, Pa
ϕ	porosity

Subscripts

a	absorption
e	effective
eq	equilibrium
f	fluid
H	hydrogen
s	solid
ss	stainless steel
sat	saturated
0	initial condition

wall strain development.

Spatial non-homogeneity of hydrogen storage bed upon repeated hydrogenation-dehydrogenation can be one of the major reasons behind the thermo-mechanical issues of storage devices. The design of such devices needs a comprehensive solution which nullifies these non-homogeneities leading to uniform charging and discharging of hydrogen. Application of aluminum foam with controlled spatial density can help to homogenize the distribution of storage alloy and provide due conduction path for the effective transfer of sorption heat.

Studies were reported on the sorption performance of metal hydride bed embedded with aluminium foam. However, effect of such foams on strain development of the storage container is not reported. The present study discusses the effect of spatial variation of foam density and cell size on sorption performance and wall strains of the given hydrogen storage device.

2. The physical model

Fig. 1 shows the schematic diagram of the vertically aligned hydrogen storage device with coaxial filter and annular cooling jacket. Aluminum foam with the given specification is inserted in the device and filled with $LaNi_5$ as the storage alloy. Hydrogen with high purity and given pressure is supplied to the storage device which is distributed in the bed with this coaxial filter.

As hydrogenation commences, storage intermetallics release sorption heat which is transferred to the coolant through the storage bed. As foam serves as an effective conduction path between the heat generating alloy and the coolant, the rate of heat conduction is improved.

In the meanwhile, hydride particles expand with increase in lattice volume. Upon repeated cycling during charging and discharging the hydride particles fragment and gradually settle towards the bottom. These fine powder particles agglomerate to a lumped mass after repeated charge-discharge cycles at the prevailing pressure and high temperature. This also leads to high stresses towards the bottom. The presence of aluminum foam relieves these stresses.

Sorption and development of associated stresses/strains as outlined above is an intricate occurrence and a true representation of the same is unfeasible as multiple processes take place simultaneously. Hence several assumptions have to be implemented for appropriate problem construction which is enlisted as follows.

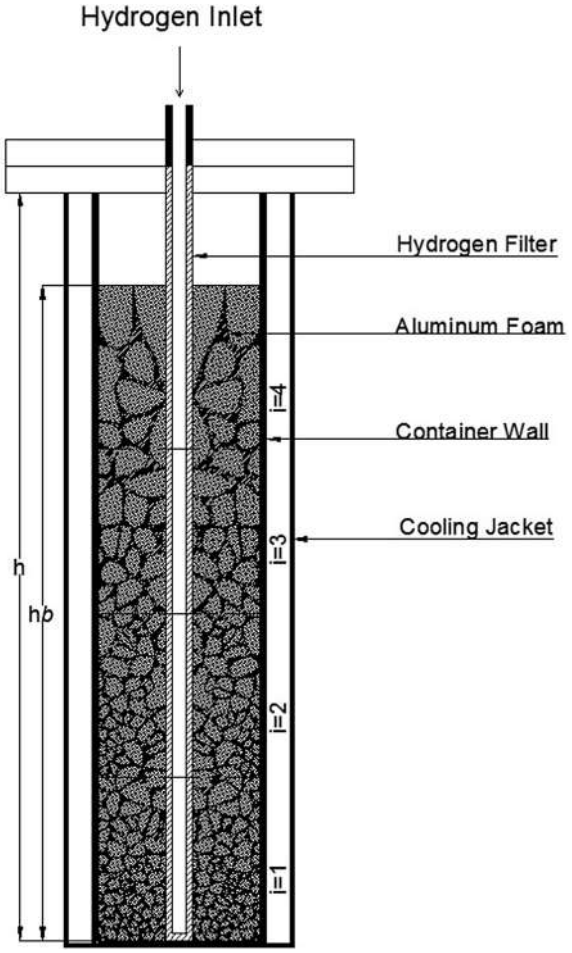

Fig. 1. Schematic of metal hydride based hydrogen storage device with central filter and annular cooling jacket embedded with aluminum foam.

1. At the moderate pressure and temperature existing in the storage bed, hydrogen behaves as an ideal gas.

2. Hydrogen sorption is only trivially affected by plateau slope and hysteresis for $LaNi_5$.
3. Only conduction can be considered as the pronounced mode of heat transfer, whereas convection and radiation turns out to be insignificant at prevailing conditions inside the hydride bed.
4. Radial variation of porosity is negligible.
5. The solid and gas exist in local thermal equilibrium within the bed.

3. Problem formulation

3.1. Mass balance of metal

As hydrogen absorb to the alloy bed, its density changes as per the following equation.

$$(1-\phi)\frac{\partial \rho_s}{\partial t} = \dot{m} \tag{1}$$

$\dot{m}$ represents the rate of hydrogen absorption.

Haque [11] proposed that an exponential relation for porosity variation depth wise would be adequate and the same is fit to the experimental data accounted by Okumura et al. Hence the porosity variation in terms of height from base (z) is given as follows.

$$\phi = Ce^{kz} \tag{2}$$

The coefficients C and k depend on bed height h_b and the corresponding porosity, φ_1. The value of C is given by the following equation.

$$\ln C + 2(\phi_1 - C) - \ln \phi_1 = 0 \tag{3}$$

and the value of k is given by

$$k = \frac{2}{h_b}(\phi_1 - C) \tag{4}$$

3.2. Sorption kinetics

The rate of hydrogen sorption in the alloy bed is given by Eqn. (5) [3].

$$\dot{m}_a = -C_a \exp\left(-\frac{E_a}{RT}\right)\ln\left(\frac{P}{P_{eq}}\right)(\rho_{sat} - \rho_s) \tag{5}$$

where C_a is reaction rate constant for absorption.

The van't Hoff equation can be utilized for the determination of equilibrium pressure as given below

$$\ln P_{eq} = A - \frac{B}{T} \tag{6}$$

where A and B are van't Hoff constants.

3.3. Energy balance

Heat conduction through the alloy bed is given by the following equation.

$$(\rho C_p)_e \frac{\partial T}{\partial t} = \lambda_e \frac{1}{r}\frac{\partial}{\partial r}\left(r\frac{\partial T}{\partial r}\right) + \lambda_e \frac{\partial}{\partial z}\left(\frac{\partial T}{\partial z}\right) - \dot{m}\Delta H^0 \tag{7}$$

Source term represents the exothermic heat during hydrogen sorption. As hydride and the gas are assumed to be in local thermal equilibrium, heat transfer between them is neglected. As the bed temperature is moderate, radiation heat transfer is also neglected.

Effective volumetric heat capacity is expressed as follows

$$(\rho C_p)_e = \phi \rho_H C_{pH} + (1-\phi)\rho_s C_{ps} \tag{8}$$

Matsushita et al. [12] put forward the following equation for the effective thermal conductivity of the hydride which combines the effect of porosity, volumetric expansion of hydride and the respective thermal conductivities of solid particle and hydrogen.

$$\lambda_e = (1-\sqrt{(1-\phi)})\lambda_H + \sqrt{(1-\phi)}\left(1 - \frac{1}{(1+\beta B)^2}\right)\lambda_s + \left(\frac{\left(1-\frac{\lambda_H}{\lambda_s}\right)(1+\beta)B}{\left(1-\frac{\lambda_f}{\lambda_s}B + \left(1-\frac{\lambda_H}{\lambda_s}\right)\beta B\right)^2}\ln\frac{1+\beta B}{(1+\beta)B\frac{\lambda_H}{\lambda_s}} - \frac{B+1+2\beta B}{2(1+\beta B)^2} - \frac{(B-1)}{\left(1-\frac{\lambda_H}{\lambda_s}B + \left(1-\frac{\lambda_H}{\lambda_s}\right)\beta B\right)(1+\beta B)}\right)\frac{2\sqrt{1-\phi\lambda_H}}{\left(1-\frac{\lambda_H}{\lambda_s}B + \left(1-\frac{\lambda_H}{\lambda_s}\right)\beta B\right)(1+\beta B)} \tag{9}$$

$$\text{where } \beta B = \left(\left(\frac{1+\varphi_p F}{1+\varphi_s}\right)^{\frac{1}{3}}(1+\alpha_0) - 1\right)B_0 \tag{10}$$

$$\varphi_s = \varphi_b F \tag{11}$$

For Equations (9)–(11), φ_P and φ_b are the expansion ratios of particle and bed respectively. β and B respectively denote the deformed factor and shape factor for hydride.

Energy balance for aluminum foam is given by the following equation:

$$\rho_{af}(c_p)_{af}\frac{\partial T}{\partial t} = \nabla\cdot\left(\lambda_{af}\nabla T\right) \tag{12}$$

3.4. Stress-strain equations

The wall stresses in the container are due to volumetric expansion and thermal expansion of hydride particles. As volume of the hydride bed increases linearly during hydrogenation [13], an effective expansion coefficient can be formulated as given below, taking into account of these two factors

$$\alpha_e = \alpha\left[1 + \alpha\Delta T + \frac{0.167}{3\alpha\Delta T}\left(1 - \left[\frac{C_{sat} - C}{C_{sat} - C_0}\right]\right)\right] \tag{13}$$

where α is the coefficient of thermal expansion for the storage alloy and C is the concentration of hydrogen in the bed.

The effective Young's modulus of the porous hydride bed can be computed using the Phani-Niyogi relation [14] as given below.

$$Y_e = Y_0\left(1 - \frac{\phi}{\phi_{cr}}\right)^p \tag{14}$$

where Y_0 is the Young's Modulus of non-porous material. ϕ and ϕ_{cr} are the actual and critical porosities respectively. 'p' is a material specific exponent.

The stress in container walls is due to the volumetric expansion of hydride bed, thermal expansion and gas pressure. The container material in the elastic regime can be represented by the equilibrium equations, strain-displacement relations and constitutive

equations. The non-linear material behaviour in the plastic regime can be represented using the Ramberg-Osgood material model [15].

$$\varepsilon = \frac{\sigma}{Y} + 0.002\left(\frac{\sigma}{\sigma_{0.2}}\right)^{n} \tag{15}$$

where $\sigma_{0.2}$ is the 0.2% proof stress and n is the strain hardening exponent defined as

$$n = \frac{\ln 20}{\ln\left(\frac{\sigma_{0.2}}{\sigma_{0.01}}\right)} \tag{16}$$

3.5. Initial and boundary conditions

The initial values of concentration, pressure and temperature of the bed are assumed to be constant and are as given below.

$$\rho_s = \rho_{s0}; \quad p = p_0; \quad T = T_0 \quad at\ t = 0, \tag{17}$$

The convective conditions existing at the annular cooling jacket removes the sorption heat and it can be represented as follows.

$$-\lambda_{SS}\frac{\partial T}{\partial r} = U\left(T_f - T\right) at\ t > 0 \tag{18}$$

At the filter tube, boundary conditions are as follows.

$$P = P_H; \quad \frac{\partial T}{\partial r} = 0\ at\ t > 0 \tag{19}$$

The hydride bed at $z = h_b$ is free to deform, while the bottom is fixed.

$$u = w = 0\ at\ z = 0 \tag{20}$$

The container wall is fixed at both ends.

$$u = w = 0\ at\ z = 0\ and\ z = h \tag{21}$$

where u and w are displacements in r and z directions respectively.

4. Methodology

In this study, four different types of foams are embedded to the metal hydride container. The density of these foams varied along the axis, as shown in Fig. 2. This is done to homogenize the strain distribution by controlling heat transfer and hydrogen sorption. The weight ratio of Al - MH used in this study is included in Table 3.

4.1. Cell structure modeling of aluminum foam

Prior to numerical simulation, computational models of hydride bed with given dimensions were modeled. As hydride bed consists of aluminum foam of intricate geometry, their modeling was done separately and as per the method proposed by Kou and Tan [16]. As per this method, given number of voronoi points were generated which is subsequently tessellated into closed polygons.

As the present study investigates the effect of foam density and its variation along the length, such foams are realized by controlled randomization of voronoi cells, as per the given equations in Fig. 2. The variation of cell area is duly addressed by offsetting the cell boundaries. While the voronoi cell generation is done with MATLAB™, spline fitting and their subsequent editing is carried out in Auto CAD™.

4.2. Numerical simulation

Once the foams of the given specifications were modeled, they are exported to COMSOL Multiphysics™ [17]. The rest of the domains which include container and storage alloy are created using the model creation features of this software. The fully coupled set of conservation equations of mass, momentum and energy along with the stress-strain equations were applied to the domains. The boundary and interface conditions as per the problem formulation are applied to the computational domain. An unstructured mesh of triangular elements of given element size and quality is generated with suitable mesh parameters. Solving the model with the given set of non-linear equations demands time-dependent, iterative solver with given solver settings. A relative tolerance of 1e-6 is fixed as the convergence criterion. Grid independence study is carried out to decide the computationally economic grid size. The numerical model is duly validated with the experimental results reported by Lin and Chen [18]. The tabulation of hoop strains at three positions along the container is given in Table 1.

The simulation results show reasonable agreement with experimental results and maximum variation of 6.25% for hoop strain at 3/8th of container height is observed. The validated computational model is used for all numerical simulations presented in this study.

5. Results and discussion

With optimum hydrogen repository features such as rapid reaction rate and excellent cyclic life, $LaNi_5$ is a promising hydrogen storage material. Influence of plateau slope and hysteresis is minimal for this alloy. The prime factor controlling the strain development in the container is sorption controlled volumetric expansion, which is predominantly heat transfer influenced for this alloy.

AISI 316, with its superior resistance against hydrogen embrittlement and high tensile strength throughout the operating temperature range, is one of the most feasible materials for container. Commercially available Aluminum foam made with Al 6101 offers good thermal conductivity, low density and formability to be embedded in the hydride bed.

Thermo-physical properties of $LaNi_5$, AISI 316 and Al 6101 as used in this numerical simulation are given in Table 2. The parameter constants of the storage device under this study are listed in Table 3. The simulations were conducted for hydride bed embedded with different types of aluminum foams. The relevant foam specific parameters along with the respective schematics are given in Fig. 2. The salient results of these numerical simulations on hydrogenation and consequent development of wall strains are discussed in the following paragraphs.

5.1. Effect on hydrogenation performance

Fig. 3 depicts the spatial variation of hydride bed temperature with and without aluminum foam while hydriding. During the initial phase of hydrogenation, the rate of exothermic heat generation is high which causes rapid rise in bed temperature. Later, the reaction rate is controlled by heat transfer through the wall to the coolant, leading to its gradual decrease. For either case, large thermal gradient can be observed near the wall and high bed temperature is prevalent near the axis. This is attributed to the low thermal conductivity of metal hydride bed. Aluminum foam improves this, leading to better transfer of heat and thereby reduces the bed temperature as observed in this figure.

(a) Sectional View of Aluminum Foam at Different Segments Along the Bed

Segment	i =1	i =2	i =3	i =4
Sectional view of aluminum foam embedded to the hydride bed	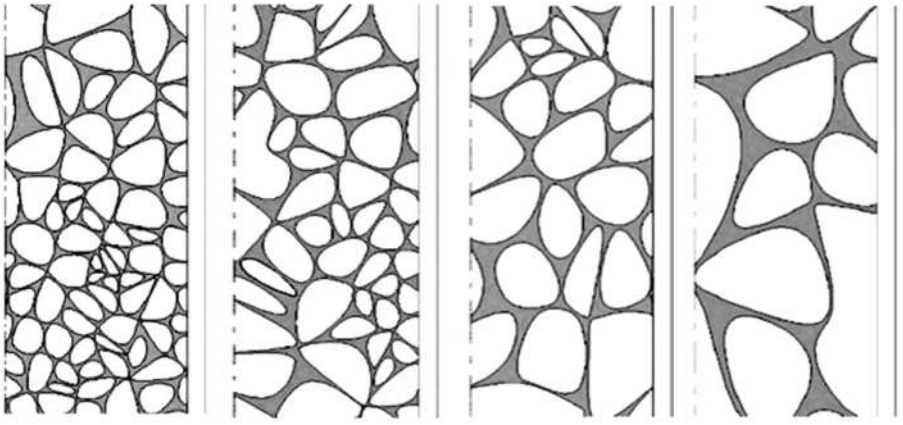			
Foam type	Foam type 4			
Al content (Wt. %)	28.4	24.86	21.25	17.4
Wt. Ratio of Al to MH	0.69	0.64	0.60	0.54

(b) Sectional View of Aluminum Foam for Different Foam Types

Foam type	Foam type 1	Foam type 2	Foam type 3	Foam type 4
Sectional view of aluminum foam embedded to the hydride bed	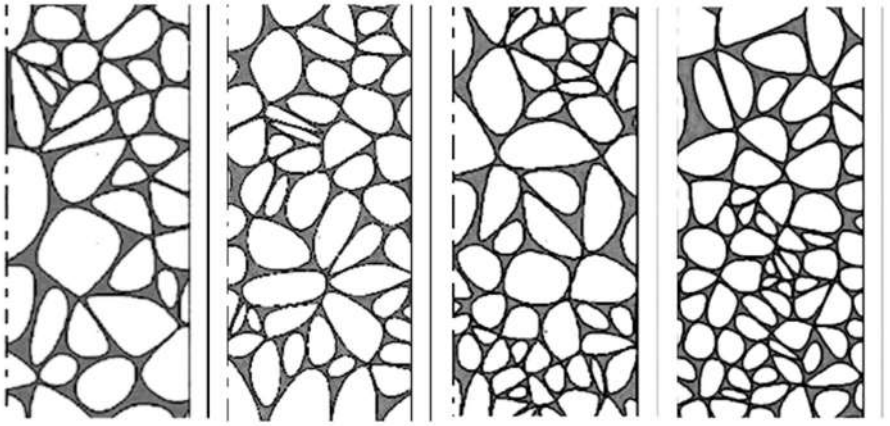			
Density of foam $\rho_{af}(z)$	450.9	-2056 z + 592.9	-2350 z + 670.1	-3953 z + 867.5
Al content (Wt. %)	16.7	21.05	23.02	28.4
Wt. ratio of Al to MH	0.358	0.468	0.525	0.696

Fig. 2. Sectional view of aluminum foam a) at different segments along the bed for foam type 4 b) at segment, i = 1 for different foam types.

Table 1
Hoop strain at different locations along the storage container.

Section (Fraction of total height)	Simulation (μm/m)	Experiment (μm/m)	Variation (%)
V1 = 1/8	17000	17500	3%
V2 = 3/8	15000	15200	1.32%
V3 = 5/8	4500	4800	6.25%

Table 2
Thermo-physical properties of materials [18–21].

Property	$LaNi_5$	Hydrogen (at NTP)	AISI 316	Al 6101
Density, kgm^{-3}	8200	0.0838	8000	2700
Specific Heat, C_p, J $kg^{-1}K^{-1}$	419	14.890	468	900
Thermal Conductivity, $Wm^{-1}K^{-1}$	20	0.1825	13.4	160
Activation Energy (abs), $Jmol^{-1}$	21170	–	–	–
Constants in kinetics equation				
Ca, s^{-1}	59.187	–	–	–
A	12.99	–	–	–
B	3704.59	–	–	–
Modulus of elasticity, Y, GPa	140	–	204	68.9
Poisson's Ratio	0.31	–	0.3	0.33
Co-eff. of Thermal Expn., α_t, $mm^{-1}K^{-1}$	1.23e-5	–	1.8e-5	2.36e-5
Yield Strength, MPa			220	170
Porosity at the top section of bed, ϕ_1	0.7			
Bed Expansion ratio, φ_b (Eqn. (11))	0.167	–	–	–
Particle expansion ratio, φ_p (Eqn. (10))	0.273	–	–	–
Exponent, p (Eqn. (14))	2.1	–	–	–

Table 3
Parameter ranges used in the study.

Parameter	Value
Bed height, (mm)	
With Al foam	98
Without Al foam	78.5
Initial temperature of hydride bed, T_0 (K)	300
Hydrogen supply pressure, P_H (bar)	15
Coolant temperature, T_f (K)	300
Heat transfer co-eff. at coolant side, U ($Wm^{-2}K^{-1}$)	500
Bed thickness, b (mm)	10
Thickness of container (mm)	1
Weight ratio of Al-Metal Hydride (MH)	0.713–0.756

In addition to the radial variation, temperature also varies along the length as shown in Fig. 4. This is due to densification of hydride by pulverization and their gravity settling leading to higher heat generation during hydrogen sorption. This causes the temperature to increase towards the bottom of the container. This is predominant for the bed with the alloy alone. Aluminum foam effectively regulates the heat transfer leading to more even temperature distribution along the bed.

Fig. 5 shows the variation of average temperature of hydride bed embedded with different types of aluminum foam during hydrogenation. As reported by several investigators [1], bed temperature increases drastically during the initial time period due to fast sorption kinetics followed with its progressive decrease due to heat exchange. Presence of aluminum foam drastically enhances this due to reasons stated above. However the effect of foam type on average bed temperature is not significant.

Fig. 6 shows the spatial variation of hydride concentration with and without aluminum foam during hydrogenation. As reported by different investigators [1], saturated alloy with higher concentration can be observed as a reaction front, which progresses towards the axis with time. This is due to the already known fact that, better heat transfer rate near the wall improves sorption rate. Better hydrogenation rate is also observed towards the top regions of the lone bed where thicker regions of saturation are evident. This can be better represented in Fig. 7 which plots the variation of average hydride concentration against container height for the bed with and without aluminum. This can be due to lower heat generation in these less dense upper regions. For the bed embedded with aluminum, improved heat regulation decreases this effect leading to more uniform hydride concentration along the length.

Presence of aluminum foam drastically improves the hydrogenation rate by improving heat dissipation. Fig. 8 shows the effect of different types of foam on average hydrogen concentration. As the variation in their aluminum content across different types of foams is minimal, the difference in net hydrogenation is marginal.

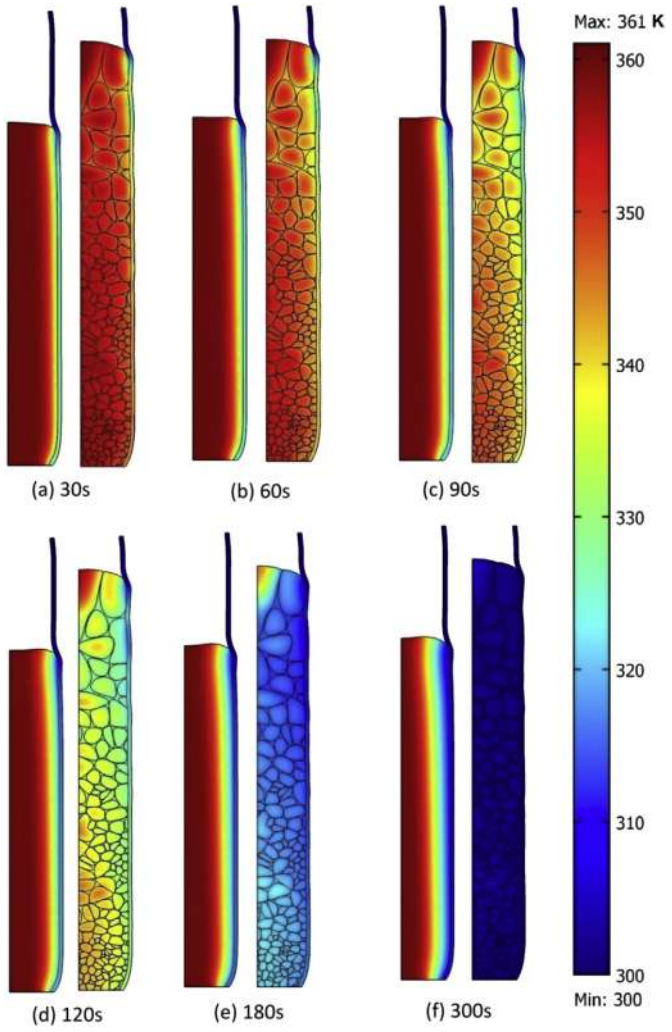

Fig. 3. Spatial variation of alloy bed temperature without foam and with foam of type 1 (uniform density) at different time intervals during hydrogenation.

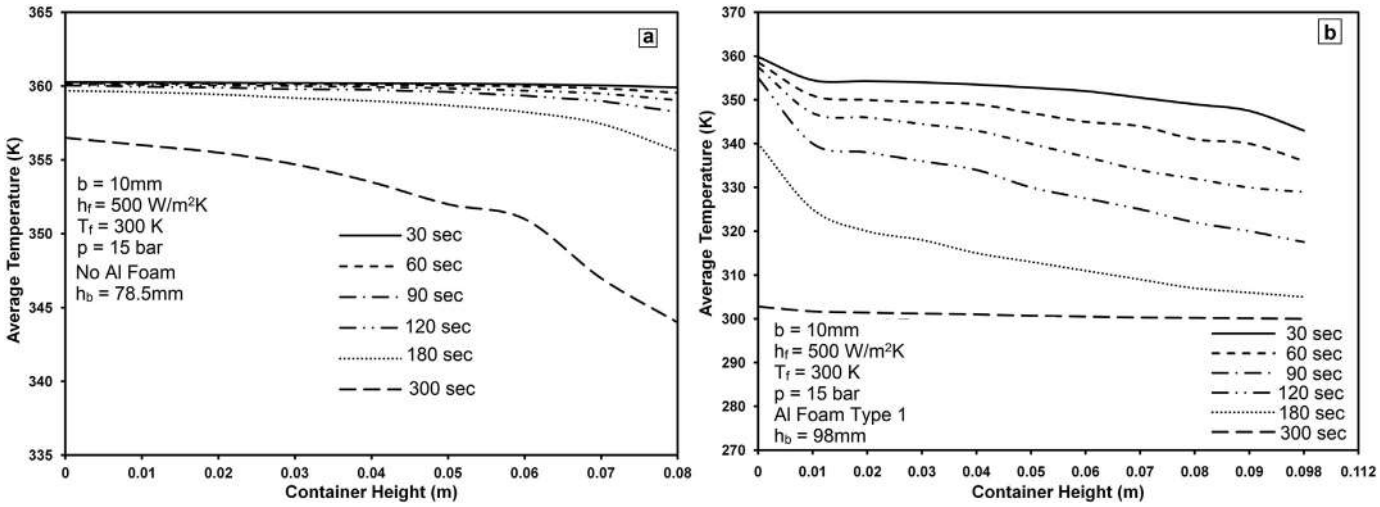

Fig. 4. Variation of average bed temperature along the vertical length of the container a) without aluminum foam b) with aluminum foam of type 1.

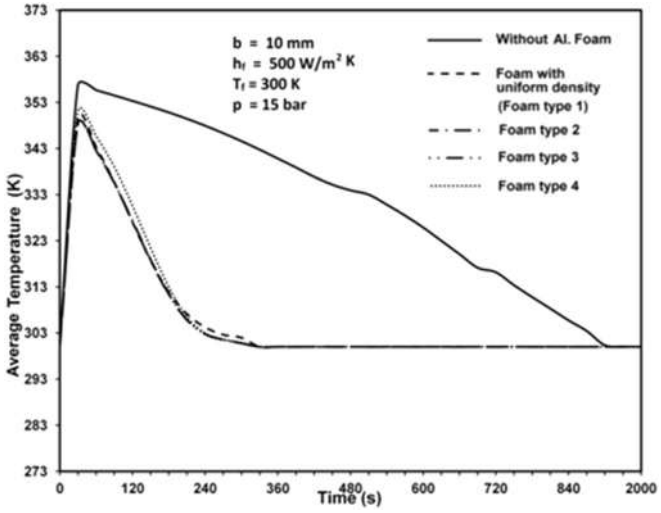

Fig. 5. Effect of aluminum foam on average hydride bed temperature.

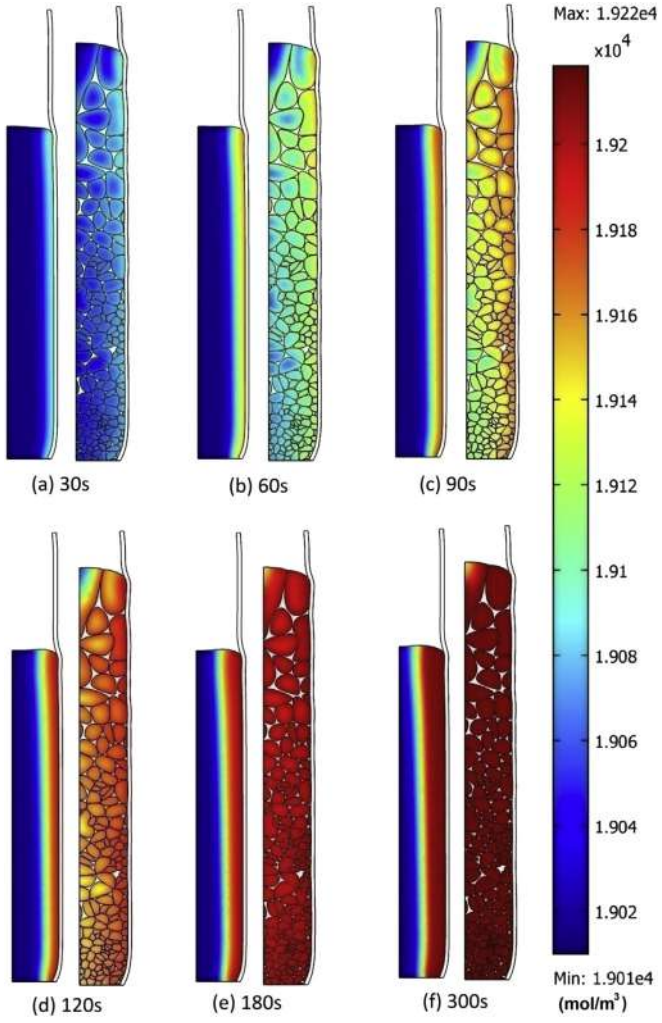

Fig. 6. Spatial variation of hydride concentration without foam and with foam of type 1 (uniform density) at different time intervals during hydrogenation.

5.2. Effect on hydrogenation strains

As hydrogen is absorbed into interstitial sites, the lattice volume increases and the metal hydride starts to expand. This exerts expansion strains onto the container body, both in circumferential and longitudinal directions. However towards the bottom of the container, the packing ratio of the metal hydride is comparatively high and the amount of stored hydrogen is consequently more. This gets reduced as we go up the container where the packing ratio decreases and consequently the strains also decrease. The effect of aluminum foam on both these types of strains is explained in the following paragraphs.

The hydrogenation strains reach the maximum at the saturation of the alloy and these strains vary with container height.

Fig. 9 shows the effect of aluminum foam on max. hoop strain vertically along the container. Peak strain is observed near the bottom where the alloy settles and agglomerates leading to higher packing. The strain gradually decreases towards the top due to decrease in packing density. The inclusion of aluminum foam reduces the peak strain and homogenizes this for the entire length. Spatially controlled foams are more effective in handling these strains where it matters most.

Fig. 10 shows the effect of aluminum foam on the max.

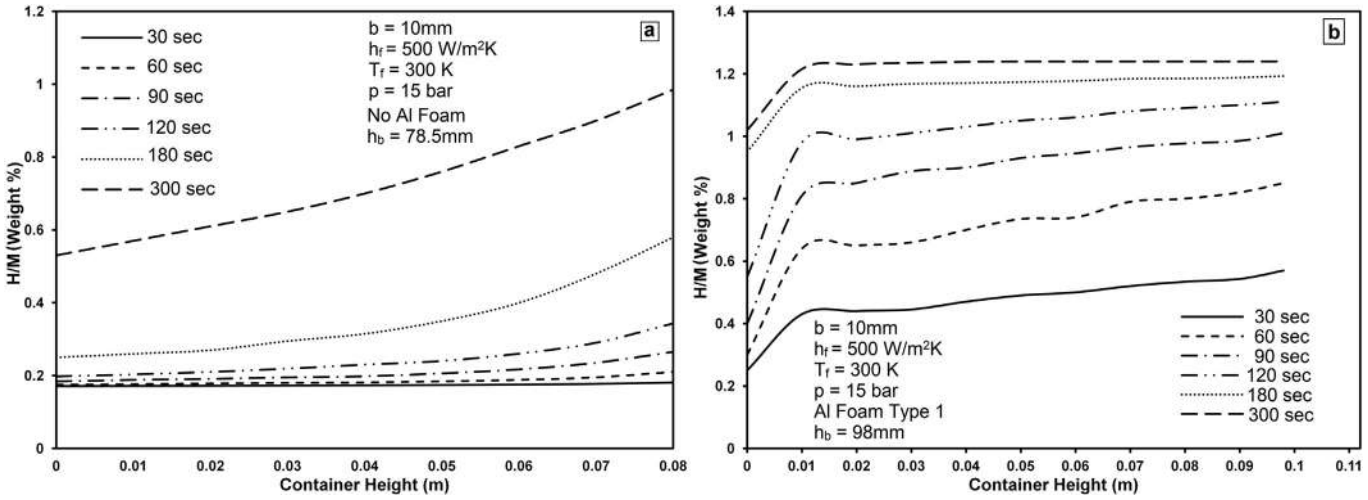

Fig. 7. Variation of hydride concentration along the vertical length of the container a) without aluminum foam b) with aluminum foam of type 1.

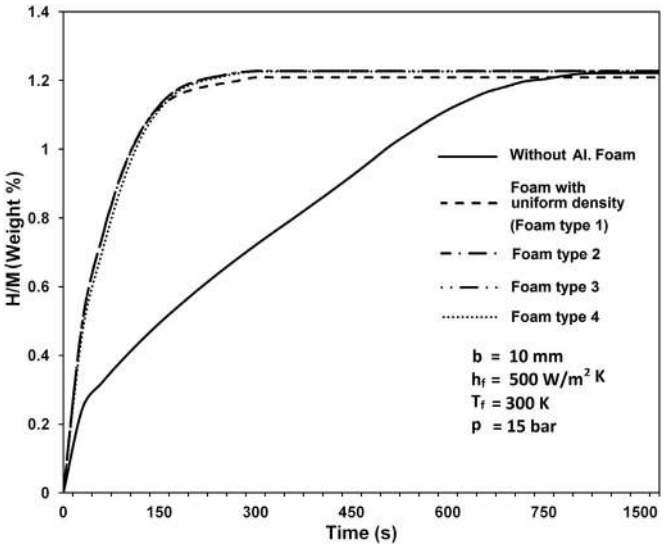

Fig. 8. Effect of aluminum foam on the hydrogen concentration during hydriding.

longitudinal strain along the container. Peak longitudinal strain is observed at the location close to the container bottom, which decreases with the presence of aluminum foam. Spatially controlled foams are found to be more effective in alleviating the strain. The longitudinal strain reverses its sign at the hydride fill limit due to discontinuity apparent at this location. This effect is found to be less drastic with the inclusion of aluminum foam.

As reported by Okumura et al. [6] the strains at 1/5th height from the bottom is found to be critical. The previous results support this, which makes the study of strains at this location for different types of foams important. Fig. 11 shows the effect of foam density variation on hoop strain at this location during hydrogenation. Progressive cell size reduction with corresponding increase in its density towards the container bottom is effective in controlling hoop strain. Foam 2 with axial variation of cell size shows marked improvement in strain reduction over the uniformly dense foam. However, later improvements by other types of foams are marginal due to their minor improvement in heat transfer. This effect is found to be less predominant in the initial phase of vigorous sorption as this is more material dependant than heat transfer controlled. However this effect is more evident in the later stages of

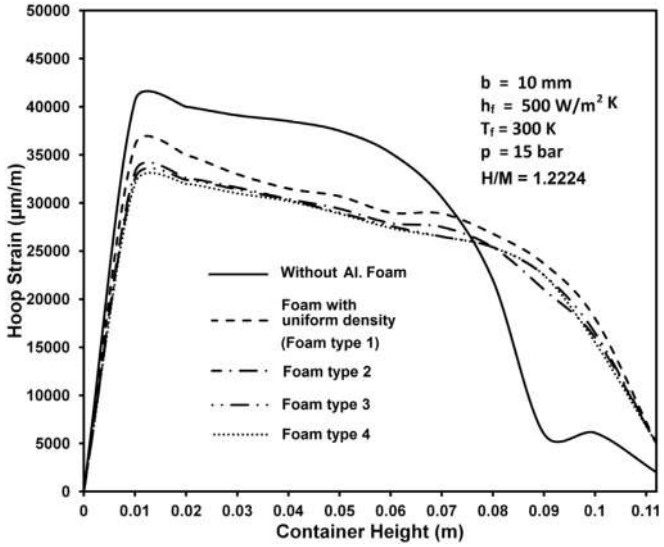

Fig. 9. Effect of aluminum foam on max. hoop strain in the container walls.

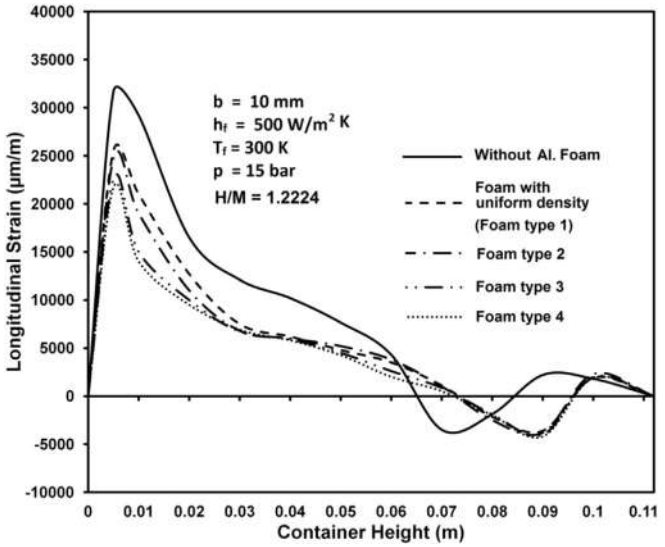

Fig. 10. Effect of aluminum foam on max. longitudinal strain in the container walls.

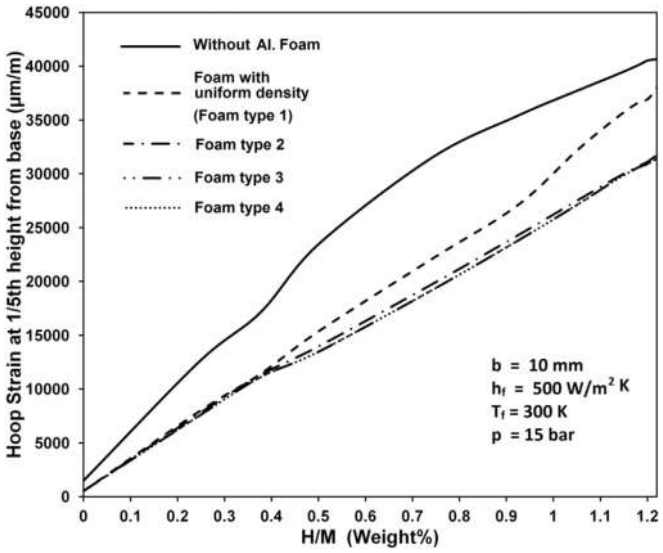

Fig. 11. Effect of Al. foam on hoop strain at 1/5th height from the container bottom.

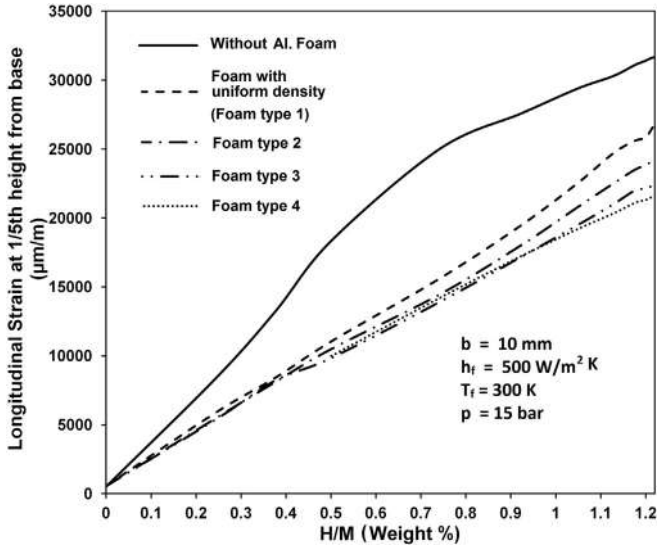

Fig. 12. Effect of Al. foam on longitudinal strain at 1/5th height from the container bottom.

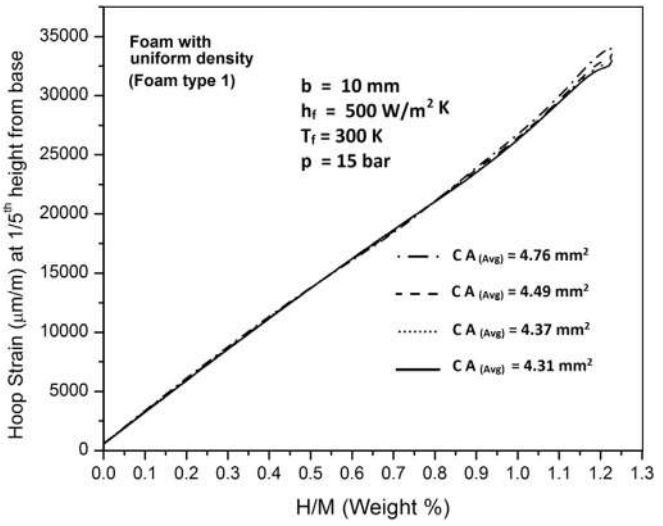

Fig. 13. Effect of cell area (CA) of the foam on hoop strain at 1/5th height from the container bottom.

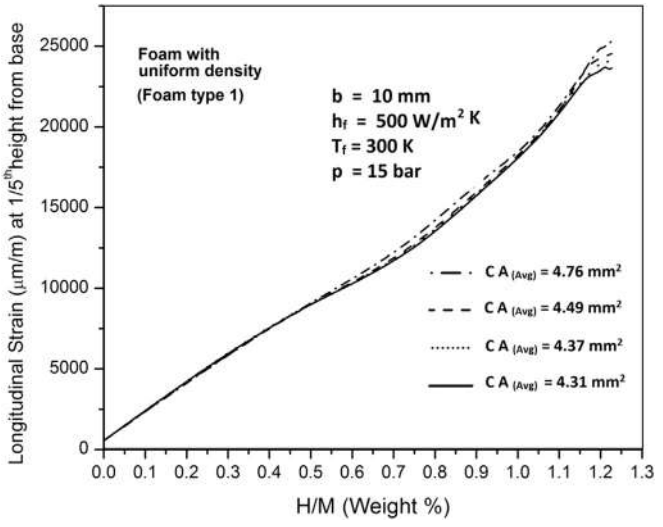

Fig. 14. Effect of cell area (CA) of the foam on longitudinal strain at 1/5th height from the container bottom.

hydrogen sorption which is thermally controlled. This leads to the important observation that the advantage of aluminum foam as a heat dissipation mechanism is more pronounced in thermally controlled sorption regime and therefore its stress reduction potential is also restricted to this regime. Similar effect can be observed for longitudinal strain as shown in Fig. 12. However their magnitude is small compared to the corresponding hoop strain.

The effect of average cell area on hoop strain and longitudinal strain for uniformly dense aluminum foams is shown in Figs. 13 and 14 respectively. Their effect is marginal in both cases. This is due to the fact that, unlike the configuration of foam, amount of aluminum is not a significant parameter that improves thermal/sorption performance and therefore do not take part in its stress control.

6. Conclusions

Numerical study of wall strain development in vertical metal hydride storage device is conducted for $LaNi_5$ based storage bed embedded with aluminum foam. Simulation results show the relevance of aluminum foam to improve thermally controlled sorption performance and reduce wall strains in these devices.

As container weight being a significant fraction of total weight of the device, hydride beds with spatially uniform performance and lower strains needs to be developed. Hydride beds embedded with foam of spatially controlled density is effective to achieve this, leading to the weight optimized design of hydrogen storage devices.

Acknowledgment

The support from Prof. S. Srinivasa Murthy and Prof. M. Prakash Maiya, Department of Mechanical Engineering, IIT Madras is gratefully acknowledged.

References

[1] S. Srinivasa Murthy, Heat and mass transfer in solid state hydrogen storage: a

review, J. Heat Trans. 134 (2012) 1–11.
[2] A. Jemni, S.B. Nasrallah, Study of two dimensional heat and mass transfer during absorption in a metal-hydrogen reactor, Int. J. Hydrogen Energy 20 (1995a) 43–52.
[3] F. Askri, A. Jemni, S.B. Nasrallah, Study of two dimensional and dynamic heat and mass transfer in a metal-hydrogen reactor, Int. J. Hydrogen Energy 28 (2003) 537–557.
[4] G. Mohan, M. Prakash Maiya, S. Srinivasa Murthy, Performance simulation of metal hydride hydrogen storage device with embedded filters and heat exchanger tubes, Int. J. Hydrogen Energy 32 (2007) 4978–4987.
[5] S.L. Garrison, B.J. Hardy, M.B. Gorbunov, D.A. Tamburello, C. Corgnale, B.A. van Hassel, D.A. Mosher, D.L. Anton, Optimization of internal heat exchangers for hydrogen storage tanks utilizing metal hydrides, Int. J. Hydrogen Energy 37 (2012) 2850–2861.
[6] M. Okumura, K. Terui, A. Ikado, Y. Saito, M. Shoji, Y. Matsushita, H. Aoki, T. Miura, Y. Kawakami, Investigation of wall stress development and packing ratio distribution in the metal hydride reactor, Int. J. Hydrogen Energy 37 (2012) 6686–6693.
[7] S.T. McKillip, C.E. Bannister, E.A. Clark, Stress analysis of hydride bed vessels used for tritium storage, Fusion Sci. Technol. 21 (2P2) (1992) 1011–1016.
[8] K. Nasako, Y. Ito, N. Hiro, M. Osumi, Stress on a reaction vessel by the swelling of a hydrogen absorbing alloy, J. Alloy. Comp. 264 (1998) 271–276.
[9] B.Y. Ao, S.X. Chen, G.Q. Jiang, A study on wall stresses induced by LaNi5 alloy hydrogen absorption-desorption cycles, J. Alloy. Comp. 390 (2005) 122–126.
[10] D. Lekshmi, G. Mohan, Numerical simulation of the parametric influence on the wall strain distribution of vertically placed metal hydride based hydrogen storage container, Int. J. Hydrogen Energy 40 (2015) 5689–5700.
[11] E. Haque, Void fraction as a function of depth and pressure drops of packed beds of porous media formed by granular material, Trans. Am. Soc. Agric. Biol. 54 (2011) 2239–2243.
[12] M. Matsushita, M. Monde, Y. Mitsutake, Predictive calculation of the effective thermal conductivity in a metal hydride packed bed, Int. J. Hydrogen Energy 39 (2014) 9718–9725.
[13] J.M. Joubert, R.C. Cerny, M. Latroche, A. Parcheron-Guegan, K. Yvon, Compressibility and thermal expansion of $LaNi_5$ and its substitutional derivatives, Intermetallics 13 (2005) 227–231.
[14] K.K. Phani, S.K. Niyogi, Young's modulus of porous brittle solids, J. Mater. Sci. 22 (1987) 257–263.
[15] W.R. Osgood, W. Ramberg, Description of Stress Strain Curves by Three Parameters, NACA Technical Note 902, National Bureau of Standards, Washington DC, 1943.
[16] X.Y. Kou, S.T. Tan, A simple and effective geometric representation for irregular porous structure modeling, Comput. Aided Des. 42 (2010) 930–941.
[17] A.B. Comsol, Comsol Multiphysics User's Guide, 2005.
[18] C.K. Lin, Y.C. Chen, Effect of cyclic hydriding-dehydriding reactions of $LaNi_5$ on the thin-wall deformation of metal hydride storage vessels with various configurations, Renew. Energy 48 (2012) 404–410.
[19] U.S. Department of Energy, Fuel cell Technologies Office, Hydrogen storage materials database, http://hydrogenmaterialssearch.govtools.us, 2017. (Accessed 4 January 2017).
[20] M. Matsushita, M. Monde, Y. Mitsutake, Experimental formula for estimating porosity in a metal hydride packed bed, Int. J. Hydrogen Energy 38 (2013) 7056–7064.
[21] M. Sahimi, Applications of Percolation Theory, Taylor and Francis, London, 1994.